Are anthropogenic aerosols responsible for the northwest Australia summer rainfall increase? A CMIP3 perspective and implications

Wenju Cai * Tim Cowan and Arnold Sullivan

CSIRO Marine and Atmospheric Research, Aspendale, Victoria, Australia

Joachim Ribbe and Ge Shi

Department of Physical and Biological Sciences, University of Southern Queensland, Toowoomba, Queensland, Australia

* *Corresponding author address:* Wenju Cai, CSIRO Marine and Atmospheric Research, PMB 1, Aspendale, Victoria 3195, Australia.

E-mail: wenju.cai@csiro.au

ABSTRACT

Severe rainfall deficiencies have plagued southern and eastern Australian regions over the past decades, where the long-term rainfall is projected to decrease. By contrast, there has been an increase over northwest Australia (NWA) in austral summer, which, if continues, could be an important future water resource. If increasing anthropogenic aerosols contribute to the observed increasing summer rainfall trend, then as anthropogenic aerosols are projected to decrease what will the likely impact be on NWA summer rainfall? This study uses outputs from 24 climate models submitted to phase 3 of the Coupled Model Intercomparison Project (CMIP3) with a total of 75 experiments to provide a multi-model perspective. The authors find that none of the ensemble averages, either with both the direct and indirect anthropogenic aerosol effect (10 models, 32 experiments), or with only the direct effect (14 models, 43 experiments), simulate the observed NWA rainfall increase. Given this, it follows that a projected rainfall reduction is not due to a projected decline in future aerosol concentrations. The authors show that the projected NWA rainfall reduction is associated with an unrealistic and overly strong NWA rainfall teleconnection with El Niño-Southern Oscillation (ENSO). The unrealistic teleconnection is primarily caused by a model Equatorial Pacific cold tongue that extends too far into the western Pacific, with the ascending branch of the Walker circulation situated too far west, exerting an influence on rainfall over NWA rather than over northeast Australia. Models with a greater present-day ENSO amplitude produce a greater reduction in the Walker circulation and hence a greater reduction in NWA rainfall in a warming climate. Therefore, the cold bias and its impact represent a source of uncertainty for climate projections.

1. Introduction

Over recent decades severe rainfall reductions have occurred in regions such as southwest Western Australia (e.g., Cai and Cowan 2006; Ummenhofer et al. 2008; Hope et al. 2009) and southeast Australia (e.g., Cai and Cowan 2008; Nicholls 2009). In contrast, austral summer (December January, February, or DJF) rainfall over northwest Australia (NWA) has increased by about 0.8% per year since 1950. Summer is the major rainfall season for the region, accounting for more than half of the annual total. If this wet season trend continues it could become an important future water resource for northern regional communities.

A point of contention is whether increasing anthropogenic aerosols have played a part in the observed rainfall increase. Comparing two sets of experiments with and without increasing anthropogenic aerosols using the CSIRO Mk3A model Rotstayn et al. (2007) suggest a possible impact from increasing Asian aerosols; this impact is achieved through an alteration of north-south surface temperature and pressure gradients in the tropical Indian Ocean. Subsequent warming in the eastern Indian Ocean induces a northwesterly monsoonal flow towards NWA. However, Rotstayn et al. (2007) describe reservations with the model that include its inability to correctly simulate interdecadal variability in Australian rainfall, and the lack of model agreement with observations over eastern Australia.

As the majority of anthropogenic aerosols are projected to decrease by the end of 21st century, including parts of Asia (Streets 2007), the inference is that, if aerosols control NWA rainfall, then long-term future rainfall over NWA will decrease. This matches projections of a future rainfall decrease over NWA by the Fourth Assessment Report (AR4) of the Intergovernmental Panel on Climate Change (IPCC), although there is significant variation in the magnitude of change among models contributing to the all-model ensemble (CSIRO 2007; Meehl et al. 2007). Shi et al. (2008) show that the modeled impact of aerosols on NWA rainfall in the CSIRO Mk3A is a consequence of the model generating an Indian Ocean Dipole (IOD) event that operates in DJF. The model also trends toward a negative IOD-like state (anomalously warm (cold) SSTs in the eastern (western) Indian Ocean) in DJF since 1950, which results in a NWA rainfall increasing trend in this season, as seen in observations. In reality, the IOD, which describes the zonal fluctuations of sea surface temperature (SST) and winds in the Indian Ocean, emerges in austral winter and terminates in late austral spring (Saji et al. 1999; Ashok et al. 2003). No IOD can survive into summer due to the onset of intraseasonal disturbances and the reversal of monsoonal winds (Rao and Yamagata 2004). However, Luffman et al. (2010) show that forcing an atmospheric model with historical tropical Indian Ocean SST trends produces a drying trend across much of northern Australia, with a small rainfall increase in central Australia. In their model, the Indian Ocean surface warming induces upper level (*surface*) divergence (*convergence*) driven by strong convective uplift, leading to suppression of convection in the surrounding regions including NWA. Other studies (Taschetto and England 2008; Zhang 2009; Berry et al. 2010) suggest the early onset and increased duration of the Australia-Asia summer monsoon may be responsible for the NWA rainfall increase. Similar observations of a prolonged monsoon have been seen in parts of central Asia (Zhang 2009). Adding to the complexity of the monsoon's influence on NWA rainfall is the recently discovered El Niño-Southern Oscillation (ENSO) Modoki (Ashok et al. 2007; Wang and Hendon 2007); El Niño Modoki events have been shown to intensify NWA rainfall, particularly in January and February (Taschetto et al. 2010).

In this paper, we use outputs of the 20th century experiments from 24 models made available as part of phase 3 of the Coupled Model Intercomparison Project (CMIP3) to assess the level of consensus in terms of the impact from increasing anthropogenic aerosols. An advantage of an ensemble mean is that when aggregated over multiple models and multiple experiments, a contribution to a trend by variability is largely cancelled out because each model and experiment has its own variability, leaving mostly the response to climate change. Further, consequences arising from biases of particular models may be offset or diluted. As we will show, results from CMIP3 models suggest that aerosols play an insignificant role. We then proceed to examine the implication for future rainfall projections using 21st century future climate experiments.

2. Model experiments, reanalysis and observations

To examine if climate models produce the observed DJF rainfall trend, we analyse the 50 years (1950-1999) from multiple 20th century experiments from 24 CMIP3 models. Model names and origins are listed in Table 1. Many models have multiple ensemble members (see Figure 2), providing a total of 75 experiments. Here the ensemble mean of each model is presented. All CMIP3 models include the direct effect of anthropogenic aerosols, but only 10 models incorporate the additional indirect effect (Figure 2 details which models include indirect). Since the single-model experiments in the CSIRO Mk3A (Rotstayn et al. 2007) contain both aerosols effects, to facilitate a better comparison we have stratified the experiments into two groups, with and without the indirect effect of aerosols. We also use a multi-century control experiment (without any climate change forcing) with the CSIRO

Mk3A to assess the impact of multidecadal variability.

Linear trends of DJF rainfall are calculated for Australia over the 1950-1999 period for each of the 24 CMIP3 models, as well as for the all-model average (75 experiments), the 14-model average (43 experiments) with the direct aerosol effect only, and the 10-model (32 experiments) average with both the direct and the indirect effect. The changes are presented in percentage of climatology to take into account the fact that the climatological value over NWA could be rather different in individual models.

To examine the process responsible for future rainfall projections across NWA, we use outputs from 21st century experiments for the period 2001-2100 to examine the future rainfall change, expressed in terms of percentage change per °C of global warming. Changes in mean sea level pressure are scaled in a similar way. This way of scaling allows the comparison between different emission scenario projections (Mitchell 2003) and was been adopted by the IPCC for the AR4. We explore the potential link between future rainfall changes and present-day simulation of mean climate and teleconnection with climate drivers.

Also deployed are reanalyses from the National Centers for Environmental Prediction (Kalnay et al. 1996), observed Australian rainfall since 1900 from the Bureau of Meteorology Research Centre (Lavery et al. 1997; Jones et al. 2009), and reconstructed SST from the Hadley Centre (Rayner et al. 2003).

3. Rainfall trends from 20th century experiments

Figure 1 shows Australian summer rainfall trend maps from the observed and from the ensemble means. Several results emerge, the first of which is that none of the CMIP3 model ensemble means (Figures 1b-1d) produces the observed rainfall trend pattern of an increase in the west and a decrease in the east of Australia (Figure 1a). Secondly, although the simulation with the indirect aerosol effect (Figure 1c) is slightly closer matched to the observed than the case without indirect aerosols (Figure 1d), neither case adequately captures the observed changes, suggesting that the indirect effect has little impact. Although each ensemble produces a tendency of a weak increase in rainfall over the western half, the trend over eastern Australia is somewhat opposite to the observed. We also examine the patterns in each individual model; only 4 out of 24 models (CSIRO Mk3.5, GFDL-CM2.1, MIROC3.2 (HiRes), and UKMO HadCM3) generate a pattern that is broadly similar to the observed (not shown).

Focusing on trends over NWA (averaged over 110°E-135°E, 10°S-25°S; land points only, see Figure 1 for outline), the results are summarized in Figure 2. The uncertainty range of the trend is estimated as the standard error of the linear regression fit on the ensemble-mean data taking into account the number of ensemble members of each model. Only nine models produce a statistically significant increasing rainfall trend, although all are much weaker compared to the observed (1950-2008), which is at 0.8% per year (summer) or nearly 50% of the climatological mean since 1950. The largest model trend is generated by GFDL2.0, which does not incorporate the indirect aerosol effect, with a trend less than half of the observed. The all-model ensemble mean trend is only 0.05% per year, while the ensemble that incorporates both the direct and indirect aerosol effects shows a slightly greater trend at 0.08% per year. Of the nine models that produce an increase, six are forced with only the direct effect of aerosols (Figure 2, red circles), and three are forced with the both aerosol effects (Figure 2, blue circle).

The multi-model approach (24 models with a total of 75 experiments) should be more reliable than using any particular individual model, as the aggregation effectively removes any possible impacts from multi-decadal variability, and dilutes the impact of any biases from individual models. However, the results indicate that increasing anthropogenic aerosols in the multi-model ensemble play a negligible role in generating the observed NWA rainfall increase. More importantly, because these models that contain increasing aerosols do not replicate the observed increase, it follows that the projected rainfall reduction is not due to a projected decrease in aerosols. Questions then arise as to what processes control the future rainfall decrease as projected by the IPCC AR4, and whether the processes are realistic. This is addressed this in Section 4.

Given that the CMIP3 model ensemble result is vastly different from the result of the CSIRO Mk3A which actually produces the observed increase (Rotstayn et al. 2007), we provide a brief focus on this model. We examine outputs of the multi-century pre-industrial control experiment from the CSIRO Mk3A to examine the possible role of natural multi-decadal variability. A time series of trends over multiple 50-year periods is constructed using a sliding window, with each point representing the trend value centred over that year. Over a 50-year period, positive trends comparable to the observed in terms of total rainfall amount and percentage of climatology (Figure 3a) are entirely possible without a climate change forcing. However, this result does not insinuate that the model produces the correct physics of rainfall variability. In this model, the eastern pole of the IOD in DJF is a part of the western Pacific warm pool (Shi et al. 2008), which varies with ENSO as a consequence of a severe westerly bias of the Pacific cold tongue (Cai et al. 2003).

This spurious IOD in DJF in the CSIRO Mk3A produces a rainfall teleconnection that is opposite to the observed, and contributes to the result that aerosols could force a rainfall increase across NWA. During El Niño, the observed DJF rainfall over NWA tends to decrease, with basin-wide warming over the Indian Ocean (including the eastern Indian Ocean). This is a consequence of a well-known atmospheric teleconnection, in which a decreased Walker circulation leads to easterly anomalies (Klein et al. 1999; Alexander et al. 2002). As such, a positive eastern Indian Ocean SST anomaly (averaged over 5°-15°S, 90°-110°E) is weakly associated with a decrease in rainfall (Figure 3b). In the model, the spurious IOD produces the relationship that is directly opposite (Figure 3c): anomalously low eastern Indian Ocean SSTs are associated with anomalously high rainfall over NWA. Because of the hemispheric asymmetry of the geographic distribution of anthropogenic aerosols (the major source is the Northern Hemisphere), a greater surface cooling is generated over the northern Indian Ocean sector than over the southern Indian Ocean (Cai et al. 2007). As a combined effect of this thermal contrast and the Coriolis force, trends of northwesterly anomalies, reminiscent of those during a negative IOD, are generated over the southern tropical Indian Ocean, particularly, the Sumatra-Java coast. These wind anomalies lead to a larger warming over the eastern Indian Ocean than over the western Indian Ocean. Following the relationship shown in Figure 3c, a rainfall increase is generated over NWA. Thus, the rainfall increase in CSIRO Mk3A is generated associated with the DJF IOD and the rainfall teleconnection.

4. A contributing factor for the projected rainfall decrease

What then contributes to the projected rainfall decrease? It is recognized that anthropogenic climate change signals project onto existing natural variability modes (Stone et al. 2001), like the Southern Annular Mode (Marshall 2003) and the IOD (Cai et al. 2009b), leading to enhanced impacts on the climate (e.g., rainfall) over many regions of Australia. Thus it is appropriate to examine whether the degree of realism in the simulation of the associated rainfall teleconnection has contributed to the projected rainfall decrease in summer.

To this end, using outputs from one experiment of each model, we have examined the summer NWA rainfall teleconnection with an important climate mode impacting this region, ENSO, by regressing grid-point detrended rainfall anomalies onto a detrended ENSO index represented by SST anomalies averaged over the NINO3.4 region (5°S-5°N, 170°W-120°W). To gauge the significance of the ENSO-NWA rainfall teleconnection we correlate grid-point detrended rainfall anomalies with the ENSO index. The maps of regression and correlation coefficients are then averaged. Compared with the observed, the biggest correlations in the all-model average are recorded over NWA (Figure 4a). These correlations are significant at the 95% confidence level, for which a 50-year sample size requires a correlation coefficient greater than 0.28. In reality, ENSO's influence on rainfall predominantly occurs over northeast Australia rather than NWA only (Figure 4b). The models perform reasonably well at capturing the rainfall teleconnection over western NWA, however they struggle to simulate ENSO's control over northeastern Australia rainfall. This means that during El Niño, simulated rainfall over NWA decreases, instead of the concurrent stronger reductions expected over northeastern Australia.

Is the strength of the ENSO-NWA rainfall teleconnection relevant to the future NWA rainfall changes? It turns out to be highly relevant, as illustrated by a scatter plot of inter-model variations of NWA DJF rainfall changes averaged over NWA for the 2001-2100 period versus inter-model variations of the ENSO-NWA rainfall correlation between time series of rainfall averaged over NWA and NINO3.4 (Figure 5). We include only 23 models because PCM1's future rainfall change is not available. The teleconnection over NWA for each model (the observations are represented by a blue line) confirms that many of the models produce too strong a correlation. Further, there is a tendency for models with a greater teleconnection to generate a greater future NWA rainfall reduction. Such a tendency, as measured by the linear fit, is statistically significant at the 95% confidence level (correlation greater than 0.41). What this result means is that a realistic simulation of the present day rainfall teleconnection has a bearing on rainfall projections for the region.

Is the bearing a part of a spatially coherent influence of the ENSO-rainfall teleconnection on the rainfall projection? To address this issue, we construct grid-point rainfall correlation with ENSO $C(x, y, k)$ and ENSO rainfall signal-to-noise ratio $R(x, y, k)$; with k representing each of the 23 models. The field of $C(x, y, k)$ is obtained by correlating NINO3.4 with grid-point rainfall anomalies. The ENSO rainfall "signal" is defined as the standard deviation of rainfall anomalies associated with ENSO, and is determined from a linear regression onto NINO3.4, and "noise" as the standard deviation of the residual after removing ENSO-related rainfall signals. As expected, a large ratio indicates that the ENSO signal is able to manifest from the background noise; therefore, the greater the ratio, the stronger the ENSO-rainfall teleconnection. We then correlate future rainfall change $FRC(x, y, k)$ (again k representing each of the 23 model) with $C(x, y, k)$ and $R(x, y, k)$ with respect to k. This is the same as calculating the correlation coefficient of the linear fit shown in Figure 5, except that this is carried out over all grid points.

The result, shown in Figure 6, highlights several important features. Firstly, the influence of the ENSO-rainfall teleconnection, or the ENSO rainfall signal-to-noise ratio, on the rainfall projection is strongest over the eastern Indian Ocean and the western Pacific encompassing NWA. The well-defined pattern underpins the systematic nature of the influence by the rainfall teleconnection or the signal-to-noise ratio. Secondly, the stronger the ENSO-rainfall teleconnection or the ENSO signal-to-noise ratio, the greater the future rainfall reduction, consistent with Figure 5.

Because the ENSO-NWA rainfall teleconnection is unrealistically strong, it follows that the projected rainfall reduction is also unrealistically strong. What drives the unrealistic teleconnection? An important contributing factor is the well-known model Pacific cold tongue and warm pool, that extends too far west into the eastern Indian Ocean and the west Pacific (e.g., Davey et al. 2002). As a consequence of this bias, the ascending branch of the Walker circulation also extends too far west (Cai et al. 2009a). As the Walker circulation oscillates with the model's ENSO cycle, i.e., shifts eastward and weakens during El Niño, an ENSO-NWA rainfall relationship is generated (e.g., see Figure 3 of Cai et al. (2009a)), in addition to unrealistic climatological rainfall (Lin 2007). This is rather problematic, because in reality, the largest teleconnection operates over northeast Australia (Figure 4b).

Why do models with a greater ENSO-NWA rainfall teleconnection produce a greater NWA future rainfall reduction? Previous studies have shown that the Walker circulation weakens in a warming climate (e.g., Vecchi et al. 2006). As the global warming signals tend to project onto existing modes of natural variability (Stone et al. 2001), one expects that models with a greater ENSO amplitude will also show a greater weakening in the Walker circulation. This is indeed the case as shown in Figure 7. We note that although the majority of models do produce a weakening of the Walker circulation, not all models do so; for example, there are four models that show a considerable strengthening of the Walker circulation (GISS-AOM, GISS-ER, INGV-ECHAM4, ECHO-G), i.e., a La-Niña like state. If we regard these four models as outliers and exclude them, the models that simulate a greater weakening in the Walker circulation tend to also produce a greater future rainfall reduction over NWA (figure not shown), where the model Walker circulation has an impact. This relationship should predominantly occur over northeast Australia rather than NWA if the models simulate the observed ENSO-rainfall teleconnection.

5. Conclusions

The hypothesis that the observed increasing summer rainfall trend over NWA is a result of increasing anthropogenic aerosols is one that is still yet to be conclusively tested. This study uses outputs of 24 models with a total of 75 experiments to provide a multi-model perspective. We find that none of the CMIP3 ensemble averages over experiments with both the direct and indirect anthropogenic aerosol effect included (10 models), or only the direct aerosol effect (14 models), simulate the observed rainfall increase over NWA. Given this, it follows that the projected rainfall reduction in these models is not due to a projected decline in future aerosol concentrations. We then proceed to address what processes may contribute to the projected rainfall decrease. We find that the projected reduction is at least in part associated with an unrealistic rainfall teleconnection that is too strong. Previous studies have shown that this unrealistic feature arises from a common model Pacific cold tongue/warm pool bias. As a consequence of the bias, the warm pool, the mean convection centre, and the associated ascending branch of the Walker circulation are situated too far west, such that their longitudinal fluctuations with the model ENSO cycle generate a rainfall teleconnection greatest over NWA rather than northeast Australia. Under global warming, the weakening in the Walker circulation is generally greater in models with a greater ENSO amplitude, as some of global warming signals project onto ENSO. It is these models with a greater ENSO amplitude, a greater NWA rainfall teleconnection, and a future weakening of the Walker circulation that also produce a greater future NWA rainfall reduction. Our study suggests that a realistic simulation of the ENSO-NWA rainfall teleconnection is essential for reducing uncertainty of rainfall projections for the region, and that the Pacific cold tongue/warm pool bias is one such uncertainty source that needs to be alleviated.

Acknowledgments.

This work is supported by the Australian Department of Climate Change. We recognize the many modelling groups that have submitted output to the Program for Climate Model Diagnosis and Intercomparison that has produced the CMIP3 database. We also thank Peter van Rensch for his assistance in producing some of the figures.

REFERENCES

Alexander, M. A., I. Bladé, M. Newman, J. R. Lazante, N.-C. Lau, and J. D. Scott, 2002: The atmospheric bridge: The influence of ENSO teleconnections on air-sea interaction over the global oceans. *J. Climate*, **15**, 2205–2231.

Ashok, K., S. K. Behera, S. A. Rao, H. Weng, and T. Yamagata, 2007: El Niño Modoki and its possible teleconnection. *J. Geophys.Res.*, **112**, C11007, doi:10.1029/2006JC003798.

Ashok, K., Z. Guan, and T. Yamagata, 2003: Influence of the Indian Ocean Dipole on the Australian winter rainfall. *Geophys. Res. Lett.*, **30**, 1821, doi:10.1029/2003GL017926.

Berry, G., M. Reeder, and C. Jakob, 2010: Summer-time rainfall over north-western Australia. *J. Climate*, in press.

Cai, W., M. A. Collier, H. B. Gordon, and L. J. Waterman, 2003: Strong ENSO variability and a super-ENSO pair in the CSIRO Mark 3 coupled climate model. *Mon. Weather Rev.*, **131**, 1189–1210.

Cai, W. and T. Cowan, 2006: SAM and regional rainfall in IPCC AR4 models: Can anthropogenic forcing account for southwest Western Australian winter rainfall reduction? *Geophys. Res. Lett.*, **33**, L24708, doi:10.1029/2006GL028037.

Cai, W. and T. Cowan, 2008: Dynamics of late autumn rainfall reduction over southeastern Australia. *Geophys. Res. Lett.*, **35**, L09708, doi:10.1029/2008GL033727.

Cai, W., T. Cowan, M. Dix, L. Rotstayn, J. Ribbe, G. Shi, and S. Wijffels, 2007: Anthropogenic aerosol forcing and the structure of temperature trends in the southern Indian Ocean. *Geophys. Res. Lett.*, **34**, L14611, doi:10.1029/2007GL030380.

Cai, W., A. Sullivan, and T. Cowan, 2009a: Rainfall Teleconnections with Indo-Pacific Variability in the WCRP CMIP3 Models. *J. Climate*, **22**, 5046–5071.

Cai, W., A. Sullivan, and T. Cowan, 2009b: Climate change contributes to more frequent consecutive positive Indian Ocean Dipole events. *Geophys. Res. Lett.*, **36**, L23704, doi:10.1029/2009GL040163.

CSIRO, 2007: Climate Change in Australia. Tech. rep., CSIRO and Bureau of Meteorology.

Davey, M. K., et al., 2002: STOIC: a study of coupled model climatology and variability in tropical ocean regions. *Clim. Dyn.*, **18 (5)**, 403–420.

Hope, P., B. Timbal, and R. Fawcett, 2009: Associations between rainfall variability in the southwest and southeast of Australia and their evolution through time. *Int. J. Climatol.*, doi:10.1002/joc.1964.

Jones, D., W. Wang, and R. Fawcett, 2009: High-quality spatial climate data-sets for Australia. *Australian Meteorological and Oceanographic Journal*, **58**, 233–248.

Kalnay, E., et al., 1996: The NCEP/NCAR 40-Year Reanalysis Project. *Bull. Amer. Meteor. Soc.*, **3**, 437–471.

Klein, S. A., B. J. Soden, and N.-C. Lau, 1999: Evidence for a tropical atmospheric bridge. *J. Climate*, **12**, 917–932.

Lavery, B., G. Joung, and N. Nicholls, 1997: An extended high-quality historical rainfall dataset for Australia. *Aust. Met. Mag.*, **46**, 27–38.

Lin, J. L., 2007: The Double-ITCZ Problem in IPCC AR4 Coupled GCMs: Ocean-atmosphere Feedback Analysis. *J. Climate*, **20**, 4497–4525.

Luffman, J. J., A. S. Taschetto, and M. H. England, 2010: Global and Regional Climate Response to late 20th Century Warming over the Indian Ocean. *J. Climate*, **23**, 1660–1674.

Marshall, G. J., 2003: Trends in the Southern Annular Mode from observations and reanalyses. *J. Climate*, **16**, 4134–4143.

Meehl, G. A., et al., 2007: Global Climate Projections. In: . *Climate Change 2007: The Physical Science Basis. Contribution of Working Group I to the Fourth Assessment Report of the Intergovernmental Panel on Climate Change*, S. Solomon, D. Qin, M. Manning, Z. Chen, M. Marquis, K. B. Averyt, M. Tignor, and H. L. Miller, Eds., Cambridge University Press.

Mitchell, T. D., 2003: Pattern scaling: An examination of the accuracy of the technique for describing future climates. *Climatic Change*, **60**, 217–242.

Nicholls, N., 2009: Local and remote causes of the southern Australian autumn-winter rainfall decline, 1958-2007. *Clim. Dyn.*, doi:10.1007/s00382-009-0527-6.

Rao, S. A. and T. Yamagata, 2004: Abrupt termination of Indian Ocean dipole events in response to intraseasonal disturbances. *Geophys. Res. Lett.*, **31**, L19306, doi:10.1029/2004GL020842.

Rayner, N. A., D. E. Parker, E. B. Horton, C. K. Folland, L. V. Alexander, D. P. Rowell, E. C. Kent, and A. Kaplan, 2003: Global analyses of sea surface temperature, sea ice, and night marine air temperature since the late nineteenth century. *J. Geophys. Res.*, **108**, doi:10.1029/2002JD002670.

Rotstayn, L. D., et al., 2007: Have Australian rainfall and cloudiness increased due to the remote effects of Asian anthropogenic aerosols? *J. Geophys. Res.*, **112**, D09202, doi: 10.1029/2006JD007712.

Saji, N. H., B. N. Goswami, P. N. Vinayachandran, and T. Yamagata, 1999: A dipole mode in the tropical Indian Ocean. *Nature*, **401**, 360–363.

Shi, G., W. Cai, T. Cowan, J. Ribbe, L. Rotstayn, and M. Dix, 2008: Variability and Trend of North West Australia Rainfall: Observations and Coupled Climate Modeling. *J. Climate*, **21**, 2938–2959.

Stone, D., A. J. Weaver, and R. J. Stouffer, 2001: Projection of Climate Change onto Modes of Atmospheric Variability. *J. Climate*, **14**, 3551–3565.

Streets, D. G., 2007: Dissecting Future Aerosol Emissions: warming Tendencies and Mitigation Opportunities. *Climatic Change*, **81**, 313–330.

Taschetto, A. S. and M. H. England, 2008: An analysis of late 20th Century trends in Australian rainfall. *Int. J. Climatol.*, **29**, 791–807.

Taschetto, A. S., R. J. Haarsma, A. Sen Gupta, C. C. Ummenhofer, K. J. Hill, and M. H. England, 2010: Australian monsoon variability driven by a Gill-Matsuno type response to central-west Pacific warming. *J. Climate*, **23 (18)**, 4717–4736.

Ummenhofer, C. C., A. Sen Gupta, M. J. Pook, and M. H. England, 2008: Anomalous rainfall over Southwest Western Australia forced by Indian Ocean Sea Surface Temperatures. *J. Climate*, **21**, 5113–5134.

Vecchi, G. A., B. J. Soden, A. T. Wittenberg, I. M. Held, A. Leetmaa, and M. J. Harrison, 2006: Weakening of tropical Pacific atmospheric circulation due to anthropogenic forcing. *Nature*, **441**, 73–76, doi:10.1038/nature04744.

Wang, G. and H. H. Hendon, 2007: Sensitivity of Australian rainfall to inter-El Niño variations. *J. Climate*, **20**, 4211–4226.

Zhang, H., 2009: Diagnosing Australia-Asian monsoon onset/retreat using large-scale wind and moisture indices. *Clim. Dyn.*, doi:10.1007/s00382-009-0620-x.

List of Tables

Table 1. Table 1: Models identifications (IDs), and their origins.

Model ID	**Origin of model**
BCCR-BCM2.0	Bjerknes Centre for Climate Research (Norway)
CGCM3.1(T47)	Canadian Centre for Climate Modeling and Analysis
CGCM3.1(T63)	Canadian Centre for Climate Modeling and Analysis
CNRM-CM3	Centre National de Recherches Météorologiques (France)
CSIRO Mk3.0	CSIRO Marine and Atmospheric Research (Australia)
CSIRO Mk3.5	CSIRO Marine and Atmospheric Research
GFDL CM2.0	Geophysical Fluid Dynamics Laboratory (United States)
GFDL CM2.1	Geophysical Fluid Dynamics Laboratory GFDL CM2.1
GISS-AOM	Goddard Institute for Space Studies (United States)
GISS-EH	Goddard Institute for Space Studies
GISS-ER	Goddard Institute for Space Studies
FGOALS-g1.0	Institute of Atmospheric Physics (IAP) Institute of Atmospheric Physics (China)
INGV	Istituto Nazionale di Geofisica e Vulcanologia (Italy)
INM-CM3.0	Institute of Numerical Mathematic (Russia)
IPSL CM4	Institute Pierre Simon Laplace (France)
MIROC3.2(medres)	Center for Climate System Research (Japan)
MIROC3.2(hires)	Center for Climate System Research
ECHO-G	Meteorological Institute of the University of Bonn (Germany/Korea)
ECHAM5/MPI-OM	Max Planck Institute for Meteorology (Germany)
MRI CGCM2.3.2	Meteorological Research Institute (Japan)
CCSM3	National Center for Atmospheric Research (United States)
PCM	National Center for Atmospheric Research
UKMO HadCM3	Hadley Centre for Climate Prediction and Research (United Kingdom)
UKMO HadGEM1	Hadley Centre for Climate Prediction and Research

List of Figures

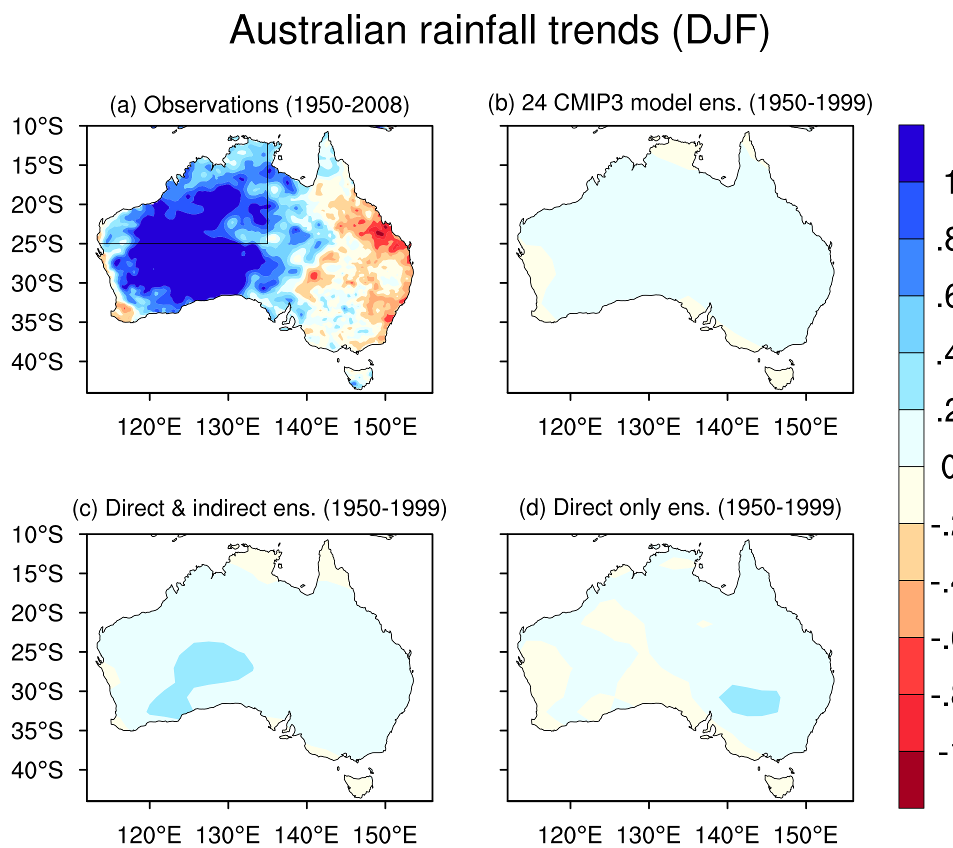

FIG. 1. Map of Australian DJF rainfall trends from (a) observations (1950-2008), (b) an ensemble mean of 24 CMIP3 models, and an ensemble mean of CMIP3 models (c) with and (d) without the indirect effect of anthropogenic aerosols. All model ensemble trends are from 1950-1999, and are expressed in % of climatology per year. Outline of NWA is shown in (a).

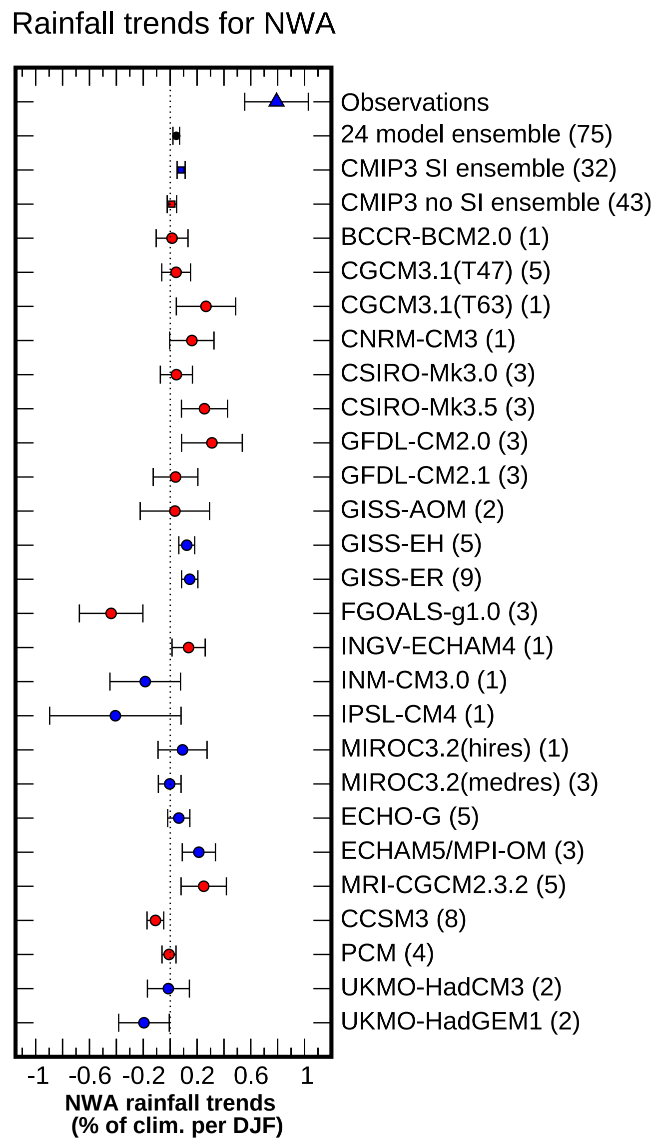

FIG. 2. DJF rainfall trends in terms of % of climatology per year from observations (1950-2008, blue triangle), and CMIP3 20th century climate model experiments (1950-1999, blue (*red*) circles indicate models with (*without*) the indirect effect of anthropogenic aerosols). The error bars indicate the standard error of the linear regression. The number of individual members in each ensemble is shown in parenthesis next the model names.

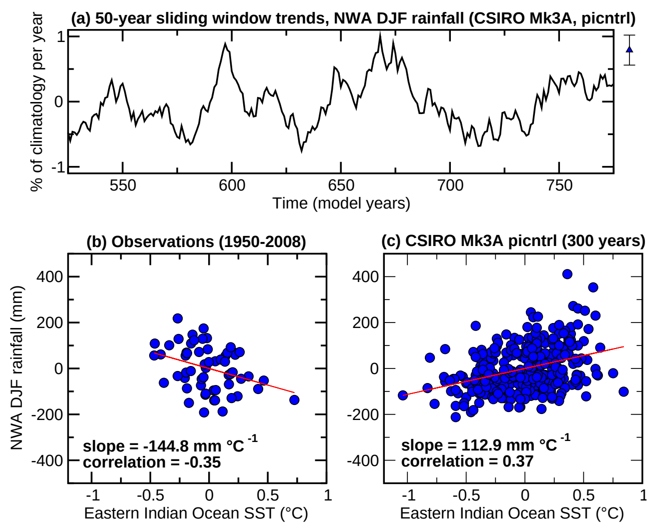

FIG. 3. (a) Time series of 50-year trends of NWA DJF rainfall calculated using a 50-year sliding window using outputs of a multi-century control experiment from CSIRO Mk3A without climate change forcing. The trend from the observations (1950-2008, blue triangle) is shown on the right side. (b) Observed eastern Indian Ocean DJF SST anomalies (averaged over 5°-15°S, 90°-110°E) against NWA rainfall. (c) The same as (b) but based on the 300-year output of a control experiment with Mk3A.

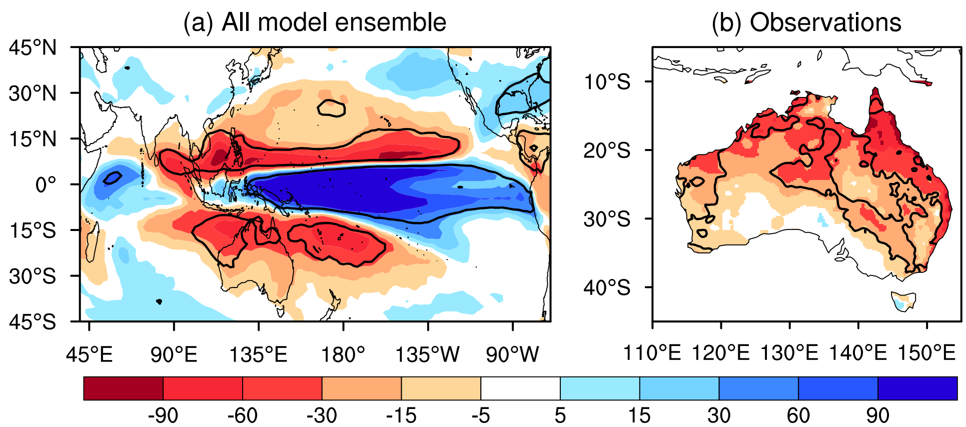

FIG. 4. Variations of DJF rainfall associated with ENSO based on (a) the 24 model average over the Indo-Pacific region, and (b) observations over Australia. The variations describe detrended gridpoint DJF rainfall anomalies regressed onto a detrended ENSO index of SSTs averaged over the NINO3.4 region (mm $^{\circ}C^{-1}$). The contours indicate statistically significant correlations at the 95% confidence level.

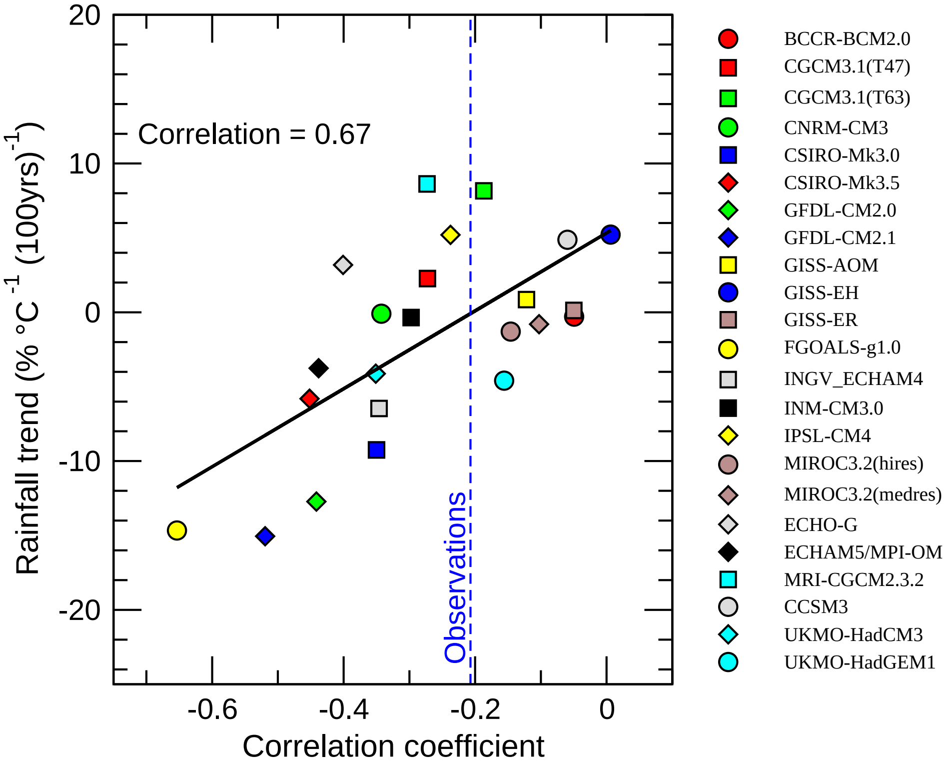

FIG. 5. Inter-model variations of NWA rainfall changes over the 2001-2100 period versus inter-model variations of the present-day ENSO-NWA rainfall teleconnection, defined as the correlation between NWA rainfall and an ENSO index in DJF for 1950-1999 (both detrended). The relationship is based on 23 models in which outputs for the future rainfall change are available. The rainfall change is expressed in % change per °C of global warming per 100-yrs to take into account the differences in model rainfall climatology and in different emission scenarios. The observed ENSO-NWA rainfall teleconnection is shown as the vertical blue line.

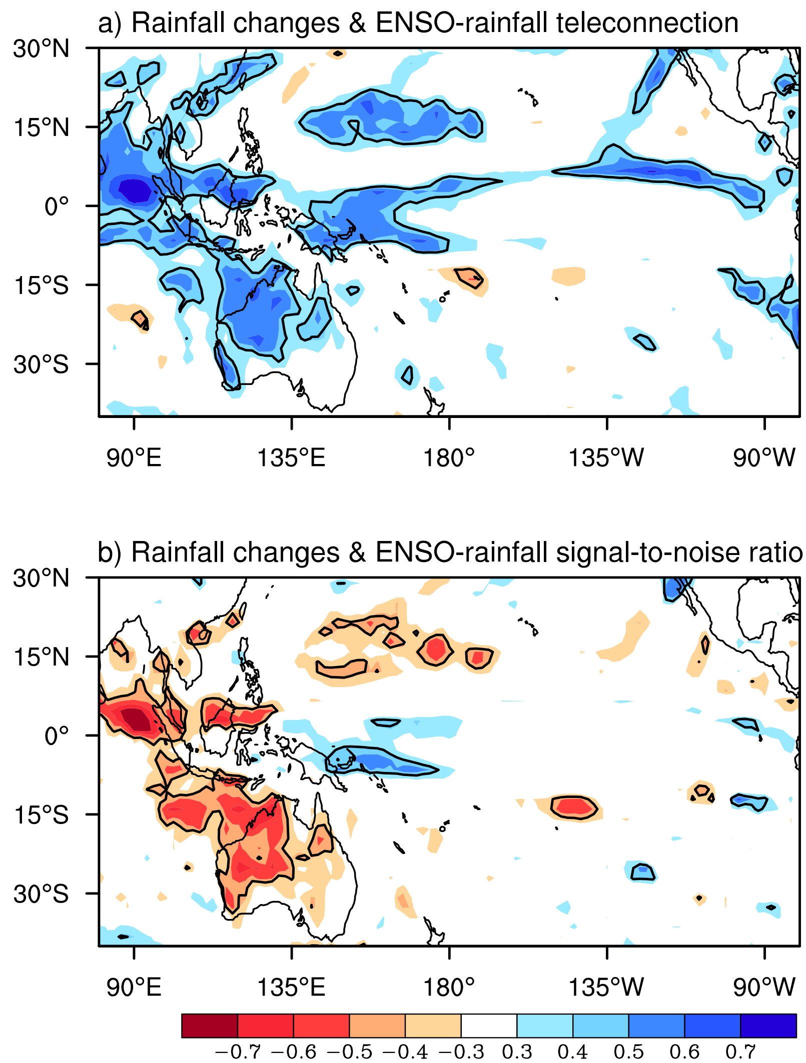

Fig. 6. Correlation of grid-point future rainfall changes over the 2001-2100 period with (a) grid-point present-day ENSO-rainfall teleconnection, and (b) present-day ENSO rainfall signal-to-noise ratio. See Section 4 for more details. The contours indicate statistically significant correlations at the 95% confidence level (an absolute value greater than 0.41).

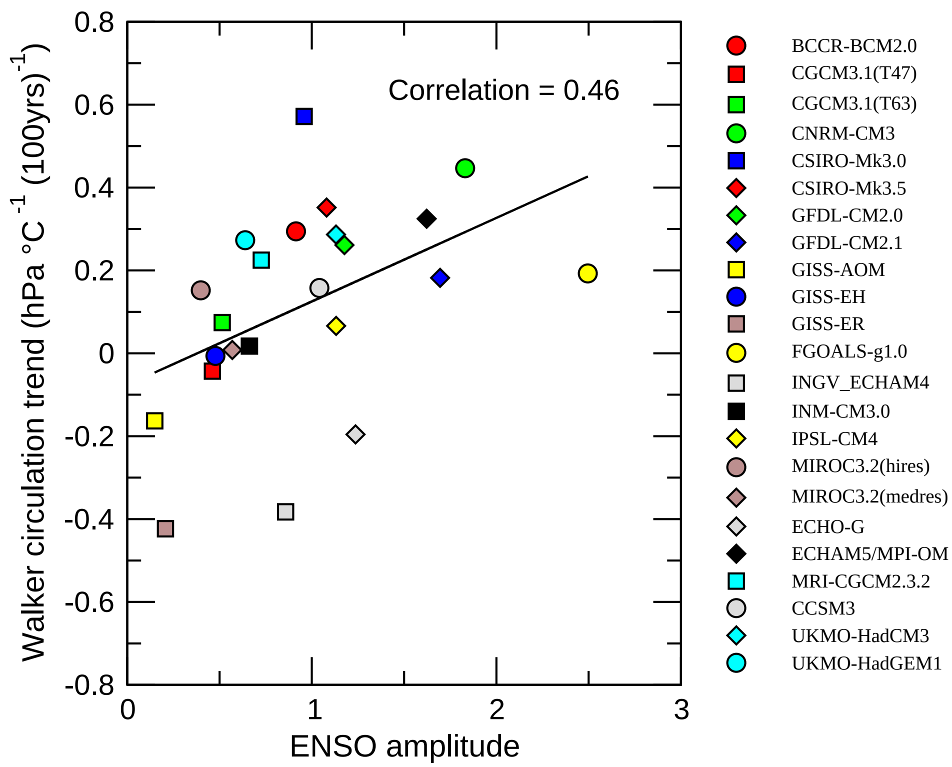

FIG. 7. Inter-model variations from 23 models of: Walker circulation changes over the 2001-2100 period versus the present-day ENSO amplitude, defined as the standard deviation of each model's NINO3.4 index for 1950-1999. The Walker circulation is defined as the difference in sea level pressure anomalies between the west Pacific (80°E-160°E, 5°S-5°N) and east Pacific (160°W-80°W, 5°S-5°N), as described in Vecchi et al. (2006). The Walker circulation change is expressed in hPa per °C of global warming per 100-yrs.